Effects of pH, Ionic Strength, Calcium, and Molecular Mass on the Arrangement of Hydrophobic Peptide Helices at the Air−Water Interface

Helen Sjögren[†,§] and Stefan Ulvenlund*[,†,‡]

Physical Chemistry 1, Lund University, P.O. Box 124, 221 00 Lund, Sweden, and AstraZeneca R&D Lund, 221 87 Lund, Sweden

Received: May 18, 2004; In Final Form: August 17, 2004

The influence of subphase characteristics (ionic strength, pH, and the presence of bridging cations) on the conformation and lateral orientation of the hydrophobic polypeptide poly-L-leucine (p-leu) has been investigated at the air−water interface with the surface film balance technique as well as with Brewster angle microscopy (BAM). In addition, Langmuir−Blodgett films of p-leu deposited on quartz and mica from different subphases have been studied by circular dichroism (CD) spectroscopy and atomic force microscopy (AFM). P-leu forms α-helices at the interface regardless of subphase characteristics. Long-range lateral orientation of the α-helical strands in the p-leu monolayer was obtained under conditions where attractive interpeptide end-group interactions prevail. These interactions were obtained under conditions where (1) end-group charges lend a zwitterionic character to the peptide, thus enabling strong electrostatic attraction between adjacent strands, (2) there is a possibility for formation of carboxylic acid dimers, or (3) calcium bridges form between carboxylate end groups. These three cases correspond to an increase of the *effective* molecular mass of the peptide. It was concluded that such an increase, and thereby an increased long-range lateral orientation, can be obtained by enabling peptide end group *attraction*, but not by screening peptide end group *repulsion*. Kinetic studies of monolayer relaxation strongly suggest that the end-group effects influence the thermodynamic, as well as the kinetic, properties of peptide monolayers.

Introduction

In recent decades, there has been an increased interest in thin films of nano-oriented structures, both in terms of fundamental science and technical applications.[1−9] A variety of different nanosized structure elements, for example, wires, rods, and tubes, have been studied.[2−5,8,10−16] Among others, nanorods arranged parallel to the substrate are useful for creating patterned arrays in sensor technology.[7] The potential technological importance of ultrathin films of synthetic polypeptides has recently been highlighted from the perspective of advanced materials, for example, optical waveguides, photo- and electron-beam resists, chemical sensors, and nonlinear optics.[17−29] Synthetic, α-helix forming polypeptides may also be a viable alternative to solid nanorods,[4,5,8] considering the fact that they display a well-defined, rigid and linear structure. α-Helical peptides are therefore interesting for their collective optical, magnetic, and electronic properties.[3,5,8] Advantages of using polypeptides as nanorods are that they are easy to synthesize and have already, as peptide models, been extensively studied and characterized at the air−water interface.[30,31] In addition, α-helices have well-defined length and width. Potential drawbacks include polydispersity and characterization difficulties.

α-Helical peptide rods spontaneously arrange at the air−water interface, because of noncovalent intermolecular interactions. The surface pressure isotherms of α-helix forming homopolyamino acids are well known. These isotherms generally display a steep rise followed by a flat plateau. The latter feature is normally interpreted in terms of a monolayer-to-bilayer transition comprising close-packed α-helical rods.[32−41] Studies have shown that long, rigid α-helical peptides form close-packed domains which partially cover the surface already at large apparent mean molecular area A_0, that is, at low surface pressures.[40,42−44]

In this study, we have investigated the effect of subphase characteristics on the surface packing of α-helical peptides. Poly-L-leucine (p-leu) with more than 100 amino acid residues was selected as model peptide. This hydrophobic homopolyamino acid comprises only aliphatic unimers, which means that the only charges on the peptide strands reside at the end groups. The pK_a for leucine in aqueous solution is 2.36 and 9.60.[45] This means that systematic variation of subphase pH and ionic strength makes it possible to investigate the effects of end-group net charge on the surface behavior of p-leu α-helices. To the best of our knowledge, the effects of the end-group net charge on the local surface orientation and film relaxation kinetics of long, hydrophobic peptides have only been studied for relatively short β-sheet forming peptides[1,6,46] and never as an effect of subphase pH. In addition, the present work deals with the influence of peptide molecular mass, subphase ionic strength, and addition of Ca^{2+} ions. Peptide packing and secondary conformation have been investigated by means of surface balance experiment and Brewster angle microscopy (BAM) as well as by circular dichroism (CD) spectroscopy, atomic force microscopy (AFM), and elemental microanalysis on peptide films deposited by the Langmuir−Blodgett (LB) technique.

Since the compression and decompression isotherms of hydrophobic peptides display pronounced hysteresis effects,[30,31] kinetics may be concluded to play a crucial role for peptide surface behavior. From a more applied point of view, proper

* To whom correspondence should be addressed. E-mail: stefan.ulvenlund@astrazeneca.com; fax: +46-46-337128.
† Lund University.
‡ AstraZeneca R&D Lund.
§ Née Gillgren.

10.1021/jp047858l CCC: $27.50
Published on Web 12/07/2004

understanding of the relaxation is essential for controlled deposition of Langmuir−Blodgett films of polypeptides. Attempts to investigate and rationalize the relaxation kinetics of homopolyamino acid films, as well as films of lipids and proteins, have been reported previously.[29,35,47−56] The present work contains a systematic investigation of the relaxation kinetics of p-leu at the air−water interface and, in particular, its dependence of subphase pH.

Materials and Methods

Chemicals. Poly-L-leucine (p-leu) was purchased from Sigma Chemicals. It was stored at −18 °C and used as received. The mean molecular weight stated by the manufacturer is 13.4 and 29.4 kDa (as determined by viscosimetry), which corresponds to an average degree of polymerization of 119 and 260, respectively. Chloroform and trifluoracetic acid (TFA) of Uvasol grade were obtained from Merck and used as received. The absence of surface active contaminants in the solvents was verified by spreading the neat solvents on clean water and 100 mM NaOH in the surface balance and then, after 15 min, recording the surface pressure upon compression. The solvents did not affect the surface pressure at any degree of compression relevant for the present study.

The solid p-leu used in this work was insoluble in all common organic solvents, except TFA. These troublesome solubility characteristics mean that chemical analysis and, in particular, purification of the starting materials are difficult. No attempts to purify the starting materials were performed in the present work. The purity was, however, verified by ^{1}H NMR experiments as previously described.[30] NMR revealed small amounts of a low-molecular weight contaminant in both p-leu samples. The area of the largest impurity signal is equal to or less than 2% of the area from the p-leu methyl groups signal. The contaminant contains only an ethyl group and it may consequently be identified as a trace of an organic solvent used in the synthesis (most likely ethanol or diethyl ether).

Cholesterol (approximately 95%) was purchased from Sigma Chemicals and used as received. All other chemicals used for subphase preparation was of pro Analysis grade and used as received.

Preparation of Spreading Solutions. Spreading solutions were prepared by first dissolving the polypeptide in pure TFA to a concentration of 20 mg/mL. These stock solutions were diluted by chloroform to yield a concentration suitable for surface balance experiments. The TFA:chloroform ratio required to prevent reprecipitation of the peptide depended on its molecular mass. P-leu with a molecular mass of 13.4 kDa gave kinetically stable, clear solutions at a ratio of 1:20, whereas the 29.4 kDa analogue required a ratio of ≥1:4. The TFA:chloroform ratio used in the surface balance experiments was, if nothing else is stated, 1:20 for 13.4 kDa p-leu and 1:4 for 29.4 kDa p-leu. The polymer concentration used in the final TFA:chloroform solutions in all surface balance experiments was 1.0 mg/mL, except for the BAM experiments, where a concentration of 0.3 mg/mL was used.

Formation of Polymer Films and Recording of Isotherms. Isotherms were recorded on a KSV 2000 System 2 surface balance equipped with hydrophilic barriers, a Wilhelmy plate made of roughened platinum, and a thermostated Teflon trough with a total surface area of 510 × 150 mm (765 cm^2) and a volume of 1.05 L. The trough was thermostated at 25.0 °C by means of a circulating water bath and enclosed in a Plexiglas box to avoid airborne contaminants. The Wilhelmy plate was oriented roughly parallel to the barriers. The subphase was prepared by use of distilled water purified on a PureLab Plus water purification apparatus and had an electrical resistivity of >18 MΩ/cm. The water was filtered through a 0.10-μm filter prior to use. Prior to the spreading of a polymer film on the subphase, the barriers were moved across the trough so that the surface area was minimized (ca. 40 cm^2), and the subphase surface was cleaned by means of a Pasteur pipet connected to a water suction pump. The barriers were then completely opened. This procedure was repeated until the surface pressure recorded at the minimum area was <0.25 mNm^{-1}. Fifty microliters of the spreading solution was added to the clean subphase surface by careful, dropwise additions from a Hamilton syringe and the solvent allowed to evaporate for at least 15 min prior to compression. The film was then symmetrically and continuously compressed. For 13.4 kDa p-leu, the effect of barrier speed on the isotherm in the range 1−10 mm/min has previously been investigated.[30] Since the barrier speed in this range has only a minor impact on the compression isotherm, all isotherms were recorded using a barrier speed of 10 mm/min.

Since pH glass electrodes are incompatible with highly acidic (pH 1) and alkaline solutions (pH 13), the subphase pH was calculated directly from the subphase composition. For alkaline systems, pH was calculated from pH = pK_w − pOH, with pK_w=14.0.

A given subphase was used for a maximum of four experiments before being discarded. In cases where measurements were possible, the pH of the subphase was monitored with a Metrohm 744 pH meter after each isotherm experiment. The pH of the subphase decreased one pH unit or less over a series of four experiments. However, this decrease did not affect the isotherms.

Recording of Kinetic Data. The kinetic measurements of film relaxation were performed using the surface balance instrumentation and sample preparation protocols described in the preceding paragraphs. Investigations of the relaxation kinetics were performed both after compression and decompression of the p-leu film. In the latter case, the film was first compressed to 65 mNm^{-1} before being decompressed to the point where the kinetics was studied. The film was compressed or decompressed (with a barrier speed of 10 mm/min) to the molecular area under investigation, where the barrier speed was set to zero and the evolution of the surface pressure followed with time. The surface pressure was recorded every other second, typically for at least 2.5 h or until the surface pressure was constant with time.

For kinetics measurements extended over long periods of time to be meaningful, the surface balance setup must, obviously, be stable with respect to external factors such as surface contamination, subphase evaporation, and temperature. The necessary stability was verified by performing a measurement of the surface pressure of a water surface left in the trough for 12 h. The results show that the background drift in surface pressure is negligible over the time scale of the kinetic measurements.

Deposition of Langmuir−Blodgett (LB) Films. Prior to LB deposition, the film under study was compressed beyond the target surface pressure, 5 mNm^{-1}, and then decompressed and kept at the target pressure for at least 20 min. Deposition was then performed by raising the substrate through the film at a speed of 3 mm/min. The substrate was oriented parallel to the barriers. All transfer ratios were in the range 0.97−1.07.

For analysis by atomic force microscopy (AFM) and scanning electron microscopy (SEM), rectangular plates of freshly cleaved

mica were used as substrates in the LB deposition. LB films for analysis by circular dichroism (CD) spectroscopy were deposited on rectangular plates (50 × 12 mm) of optic quartz. Prior to the deposition, the plates were placed in sulfochromic acid for several hours and then washed with large amounts of purified water.

Circular Dichroism Spectroscopy. CD spectra of polyamino acid LB films were recorded on a Jasco J715 spectropolarimeter. The quartz plate supporting the film was placed in the standard cuvette holder of the instrument. Two perpendicular orientations of the quartz plate were investigated to check for contributions from linear dichroism originating from long-range net lateral orientation of the polypeptide strands on the substrate.

Because of the weak CD signal from the LB films, overnight sampling (corresponding to >700 scans) was required. The low intensity of the signal also necessitated correction for the weak background contribution from the quartz substrate and minor instrument misalignment. Consequently, the CD signal from a clean quartz plate was recorded by overnight sampling and this signal was subsequently subtracted from all spectra.

Atomic Force Microscopy. Constant force AFM studies of LB films on mica were performed in contact mode on a Nanoscope IIIa instrument (Digital Instruments, Santa Barbara, CA). Experiments were run under ambient atmosphere and temperature within 10 h from sample preparation. An E tube scanner was used for imaging. Microfabricated square pyramidal shaped tips of silicon nitride with a bending spring constant of 0.12 N/m (manufacture specified, Digital Instruments, Santa Barbara, CA) were used as received. The scan rate was 2 Hz and the applied force was about 1−10 nN. Each sample was checked for tip-induced damages after scanning. The samples were scanned in two directions perpendicular to each other to secure that the image was not influenced by the scanning direction.

Images were obtained from at least 10 macroscopically separated areas on each sample. All images were processed using standard procedures for plane-fit and flattening in Nanoscope IIIa software version 5.12 (Digital Instruments, Santa Barbara, CA) without any filtering.

Brewster Angle Microscopy. The BAM images were recorded by mounting a Langmuir trough in an Optel Multiscope ellipsometer in which the light detector was replaced by a CCD camera and an objective lens was added to the detector arm. The Langmuir trough was a KSV Minitrough, (area 243.8 cm^2) equipped as the KSV 2000 trough described above. The whole assembly was placed on a vibration-isolated table.

The surface concentration in the BAM experiments was the same as that in the experiments on the larger trough. Before starting an experiment, the trough was cleaned and the sample solution was spread using the procedures described above.

BAM images were recorded before compression and continuously during the compression and decompression of the film, using a barrier speed of 6.4 mm/min, which corresponds to the same compression rate (area per monomer and time) as above.

The size of the BAM images is 570 × 760 μm, with a lateral resolution of about 1−3 μm.

Scanning Electron Microscopy. The surface characterization and elemental microanalysis was performed using a JEOL JSM-5600LV scanning electron microscope equipped with a microanalysis unit from Oxford Instruments, INCA Energy. The measurements were performed in high vacuum with an acceleration voltage of 20 kV and a 20-mm working distance, using an SEI detector. For the microanalysis, a Si(Li) detector was used. Elemental microanalyses were performed by energy-dispersive X-ray microanalysis both on areas containing aggregates and on smooth monolayer regions. In each case, three macroscopically separated areas were analyzed.

The LB film deposited onto mica was attached to the sample stub with carbon sticky tape and the surface was coated with gold in a sputter coater before analysis.

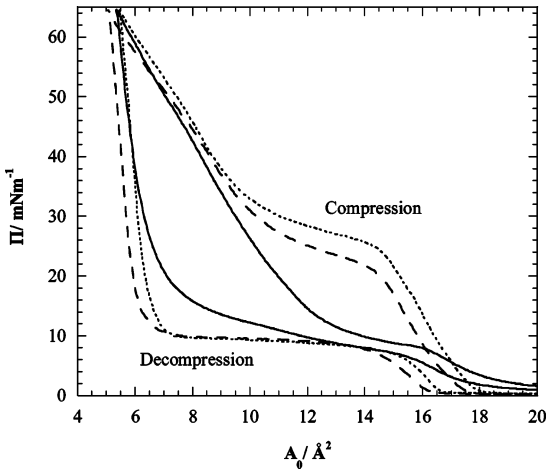

Figure 1. Compression and decompression isotherms of p-leu ($\langle M \rangle_{vis}$ = 13.4 kDa) when spread on subphases containing 100 mM NaOH (solid trace), 100 mM HCl (dashed trace), and 100 mM NaCl (dotted trace). For clarity, results only from three different pHs are shown. A comprehensive summary of all data is given in Figure 2.

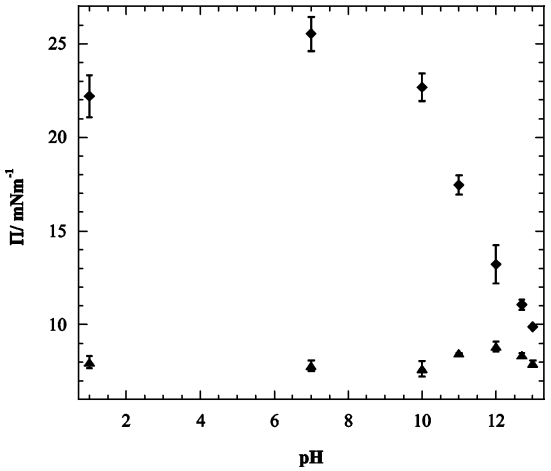

Figure 2. Surface pressure at the collapse plateau (A_0 = 14 Å) as a function of the calculated subphase pH for p-leu ($\langle M \rangle_{vis}$ = 13.4 kDa) for the compression (diamonds) and decompression (triangles) isotherms. The subphase ionic strength was kept constant at 100 mM by addition of NaCl. The data points represent the mean value from at least three independent measurements at each pH, and the error bars correspond to one standard deviation.

Results

The surface pressure isotherms displayed good reproducibility under all pH conditions, and the irreversible loss of film material upon a repeated compression/decompression cycling was very limited, even when films were compressed to very high surface pressures (65 mNm^{-1}).

Upon increasing the subphase pH from neutral to alkaline at constant ionic strength, the surface pressure at the onset of monolayer-to-bilayer transition (henceforth called the monolayer collapse plateau) in the compression isotherm decreases markedly (Figures 1 and 2). Similarly, the onset of the compression isotherm shifts toward larger apparent mean molecular area, A_0, upon increasing pH (Figure 1). Also, the surface pressure at

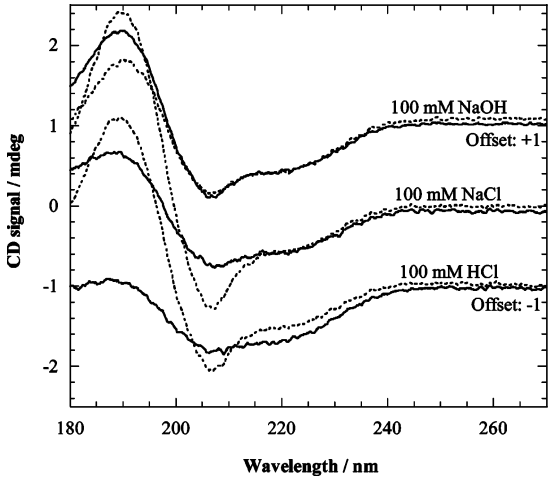

Figure 3. CD spectra of LB films of p-leu ($\langle M \rangle_{vis}$ = 13.4 kDa) deposited on quartz at Π = 5 mNm^{-1}. The samples were analyzed with the substrate in both vertical (0°, solid traces) and horizontal (90°, dotted traces) position. Prior to deposition, the polypeptide was spread onto the air−water interface on three different subphases, namely, 100 mM NaOH, 100 mM NaCl, and 100 mM HCl. For clarity, the spectra of the peptide deposited from 100 mM NaOH and 100 mM HCl have been shifted one unit along the ordinate.

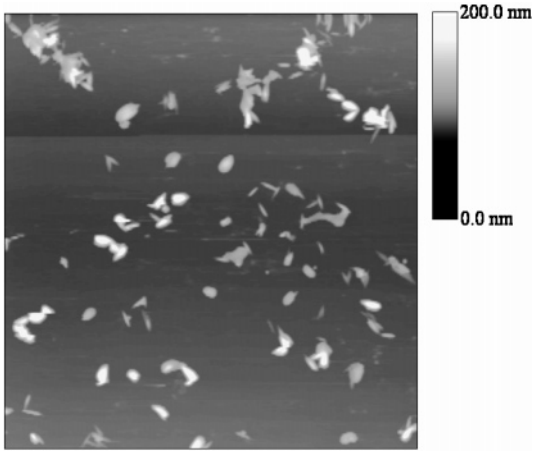

Figure 4. AFM image of an LB film of p-leu ($\langle M \rangle_{vis}$ = 13.4 kDa) spread on 100 mM NaOH and deposited on mica at Π = 5 mNm^{-1}. The dimensions of the displayed area are 15 × 15 μm.

low degrees of compression (A_0 > 17 Å^2) is substantially higher on the alkaline subphase. In effect, these observations suggest that the monolayer (prior to the collapse plateau) is more compressible at higher pH. The isotherm displays the same pH dependence (results not shown) for p-leu spread on a 100 mM carbonate buffer prepared from Na_2CO_3 and $NaHCO_3$ at pH 10, thus strongly suggesting that the observed effects are indeed general and solely attributable to the subphase pH.

In stark contrast, the isotherms show only minor pH dependence under acidic conditions (Figures 1 and 2). Even an extremely low subphase pH (1.0 M H_2SO_4), well below the acidic pK_a for p-leu (2.36), only has a minor effect on the surface pressure at the isotherm collapse plateau (results not shown).

BAM images of the monolayer before compression (A_0 > 30 Å^2) display solidlike domains much larger than the size of the BAM image (0.4 mm^2), both when 100 mM NaOH and 100 mM NaCl were used as subphase. The size of the domains makes it impossible to quantify any difference in domain size between different subphases. For both subphases studied, the domains covered a surprisingly large fraction of the surface, already at surface pressure close to zero (A_0 > 30 Å^2). However, it was observed that there were more water channels and larger areas not covered with solidlike domains when the alkaline subphase was used. The borders of the domains appeared more distinct on the neutral subphase. During film compression, collision and concomitant fusion of domains were observed on both subphases.

The fact that the BAM images display solidlike domains already at surface pressure close to zero makes it unlikely that LB transfer would result in internal film rearrangements that could, in turn, change the degree of lateral peptide orientation. At a surface pressure of 5 mNm^{-1} (where subsequent LB depositions were actually performed), the whole peptide film is solidlike, unlike (for instance) liquid-expanded/liquid-condensed systems where rearrangements during film transfer have previously been observed.[57]

As expected, the CD spectra of LB-films (Figure 3) were consistent with that of a peptide in a predominantly α-helical conformation, regardless of subphase pH.[30,31] When the samples were placed in a horizontal position, the spectra display a maximum at 192 nm, along with two minima at 208 and (less well-defined) 222 nm. The general characteristics of the CD spectra of peptide films follow those of isotropic CD spectra of peptides in solutions.[58,59] However, previous work show that CD spectra of peptide films contain appreciable contributions from linear dichroism and direct comparison with the isotropic case is therefore not possible.[31] However, the CD spectra in Figure 3 are in perfect agreement with previously published CD spectra of peptide monolayers in α-helical conformation, where the peptide conformation has been verified by LD spectroscopy and ATR−IR.[31] The CD data in Figure 3 strongly suggest that the subphase pH does not affect the secondary peptide surface conformation to any appreciable extent. The orientation of the quartz plate, on the other hand, substantially influenced the CD spectra when a neutral or acidic solution was used as subphase, but only to a minor extent in the alkaline case. In general, a pronounced angular dependence is due to a strong contribution from linear dichroism and, therefore, directly correlates with the presence of long-range net lateral orientation of the polypeptide strands on the substrate on the scale of the area analyzed in the CD experiment (4 × 8 mm). This correlation between CD angular dependence and LD has been investigated and verified elsewhere.[31,58,60] We may thus conclude that the degree of long-range order within the deposited monolayers is higher when the peptide is spread onto acidic or neutral subphases than on alkaline subphases.

To relate the CD and isotherm data to the surface morphology of 13.4 kDa p-leu monolayers, the peptide was deposited onto mica from various subphases and the surface morphology was imaged by AFM. AFM images of p-leu deposited from 100 mM NaCl and 100 mM HCl reveal smooth and featureless surfaces, while monolayers deposited from 100 mM NaOH contained particles in the submicron range, coexisting with a smooth matrix (Figure 4). This type of morphology also prevailed in films of p-leu spread on carbonate buffer at pH 10 and therefore seems to be a general effect of increasing pH. Formation of submicron particles ("aggregates") has previously been observed in monolayers of p-leu when the peptide was spread onto the air−water interface from neat TFA or solvents mixtures very rich in TFA.[30] This type of particles was concluded to consist of pure aggregated peptide. However, in these cases, the formation of particles resulted in a decrease of the amount of peptide available for film formation and it therefore went hand in hand with a substantial shift of the isotherm toward smaller areas. More specifically, A_0 at close

packing was reduced from 18.8 to 5.7 Å^2 when the spreading solvent was changed from 1:20 TFA:chloroform to pure TFA.[30] Such an isotherm shift was not observed in the present work (Figure 1), which suggests that the particles, in this case, do not comprise aggregated peptide. Nevertheless, it was judged essential to verify that the particle formation observed in films spread from TFA-containing media onto alkaline subphases was directly due to the spreading solvent (or any impurity therein) rather than to peptide aggregation. P-leu is virtually insoluble in all other solvents than TFA, and it is therefore impossible to exclude TFA from the solvent mixture used to spread this peptide onto the surface. A nonpeptide system (cholesterol) was used to investigate the general effects of TFA on LB film morphology (see Supporting Information). These data strongly suggest that (1) TFA as such leads to a formation of submicron particles in films whenever the subphase pH is high and (2) these particles do not affect monolayer characteristics to any appreciable extent.

The elemental microanalysis of LB-films of p-leu deposited on mica showed that film areas containing one or more aggregates contain fluorine, whereas areas with a smooth monolayer do not contain any detectable amounts of this element. The results thus suggest that on alkaline subphases, crystallites of trifluoroacetate salt, formed by the neutralization of TFA in the spreading solvent, deposit on top of the peptide film, effectively protecting them from dissolution.

The isotherm and CD data are, in themselves, unable to answer the question whether the observed pH effects are kinetic or thermodynamic in origin, or both. The relaxation behavior of the monolayers was therefore studied, primarily in an attempt to derive the pH dependence of the equilibrium surface pressure.

As discussed in the Introduction, the monolayer relaxation kinetics of polyamino acid monolayers on neutral subphases has been described earlier and rationalized in terms of nucleation and growth of crystalline regions. In the present work, we set out to substantiate this observation by analyzing the relaxation process in terms of the Avrami equation (eq 1) for polymer crystallization kinetics.[61−72]

$$1 - X = \mathrm{e}^{-kt^n} \tag{1}$$

Here, X is the volume fraction of crystalline material, k is the rate constant of the crystallization process, whereas the exponent n carries information about the geometry of the growing crystallites. More specifically, n is the sum of the number of dimensions of the crystallite and the order of the rate process.

To adapt the Avrami equation to the present process, we assume that the surface pressure Π of the system depends linearly on the fraction of crystalline material. Denoting the surface pressure of the crystalline and noncrystalline material Π_c and Π_n, respectively, we can then write

$$\Pi = X\Pi_c + (1 - X)\Pi_n \tag{2}$$

Substituting eq 2 into eq 1 gives

$$\Pi = \Pi_c + (\Pi_n - \Pi_c)\mathrm{e}^{-kt^n} \tag{3}$$

Further assuming that the crystallization process has not proceeded to any significant extent at the start of the kinetic measurement, we can identify Π_n as the surface pressure at $t = 0$. This leaves n, k, and Π_c to be determined from the kinetic data. Strictly speaking, it is, of course, impossible to obtain three independent parameters from a given set of data pairs by a simple least-squares refinement. However, there is a useful constraint in the present systems, namely, that the limiting surface pressure as $t \rightarrow \infty$ (Π_c) for a given system and area must (in the ideal case) be the same for the experiments conducted after compression as for those conducted after decompression.

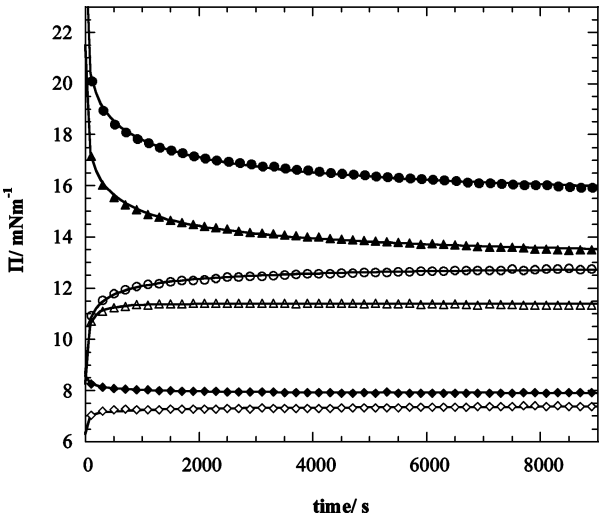

Figure 5. Surface pressure as a function of time for p-leu ($\langle M \rangle_{vis}$ = 13.4 kDa). Relaxation after compression (filled symbols) and decompression (open symbols). For clarity, only every 100th data point is shown. The target molecular area was set to 14.5 Å^2 for 100 mM NaOH (diamonds) and 12.5 Å^2 for 100 mM NaCl (circles) and 1 mM NaOH (triangles). The data were subjected to a least-squares fit to eq 3 (solid lines). The refined parameters from the fitting procedure are listed in Table 1.

The relaxation of p-leu at the collapse plateau was determined after compression and decompression for different subphase concentrations of NaOH, namely, 0, 1.0, and 100 mM (Figure 5). The ionic strength in all experiments was kept constant at 100 mM through addition of NaCl. Equation 3 was fitted to the data by standard least-squares procedures. The constraint that the refined values for the equilibrium surface pressure (Π_c) after compression and decompression should be equal was used as a check for successful fitting. However, it has to be taken into account that there is a limited loss of film material at high surface pressures and that the refined value of Π_c after decompression therefore is to be expected to be somewhat lower than after compression. Although the procedure is not strict from a mathematical point of view, it provides results that are meaningful to analyze in qualitative terms.

As is evident from the data in Figure 5 and the refined parameters in Table 1, the relaxation data show excellent agreement with the Avrami equation. This provides strong support for the idea that the film collapse comprises nucleation and growth of crystallites. The data and refined values for Π_c also clearly suggest that not only the relaxation rate but also the equilibrium surface pressure depend on subphase pH. They therefore also support the idea that the subphase pH affects the thermodynamic, as well as the kinetic, characteristics of peptide films.

Attempts were also done to study the kinetics at surface pressures below the collapse plateau (at $\Pi = 5$ mNm^{-1}). However, because of the minute changes in surface pressure with time under these conditions, these attempts proved unsuccessful.

To study the influence of electrostatics on monolayer characteristics, the effects of subphase ionic strength were studied by adding 5 M NaCl to the 100 mM NaOH and the 100 mM NaCl subphases. In the case where the peptide carries a net charge, that is, the alkaline case, we find that the subphase

TABLE 1: Results from the Least-Squares Fit of the Data in Figure 5 to Eq 3, Given as Mean Values ± the Standard Error of the Mean[a]

subphase		Π_n/mNm^{-1}	n	k	Π_c/mNm^{-1}
100 mM NaCl	compression	25.26	0.3028 ± 0.0010	0.1720 ± 0.0008	15.332 ± 0.011
100 mM NaCl	decompression	8.27	0.3291 ± 0.0011	0.1855 ± 0.0011	12.836 ± 0.003
1 mM NaOH	compression	21.51	0.3102 ± 0.0011	0.1723 ± 0.0009	13.068 ± 0.008
1 mM NaOH	decompression	8.66	0.5098 ± 0.0024	0.1295 ± 0.0016	11.383 ± 0.000
100 mM NaOH	compression	8.58	0.4542 ± 0.0020	0.0743 ± 0.0009	7.900 ± 0.000
100 mM NaOH	decompression	6.30	0.2280 ± 0.0037	0.3649 ± 0.0058	7.429 ± 0.004

[a] Π_n (the experimental surface pressure at $t = 0$) was kept constant during the least-squares refinement of n, k, and Π_c.

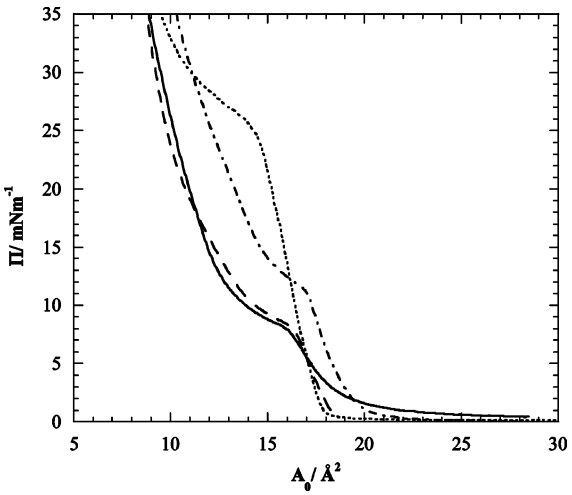

Figure 6. Surface pressure isotherms of p-leu ($\langle M \rangle_{vis}$ = 13.4 kDa). Compression isotherms when spread on 100 mM NaOH (solid trace), 100 mM NaOH + 5 M NaCl, (dashed trace), 100 mM NaCl (dotted trace), and 5 M NaCl (dashed and dotted trace).

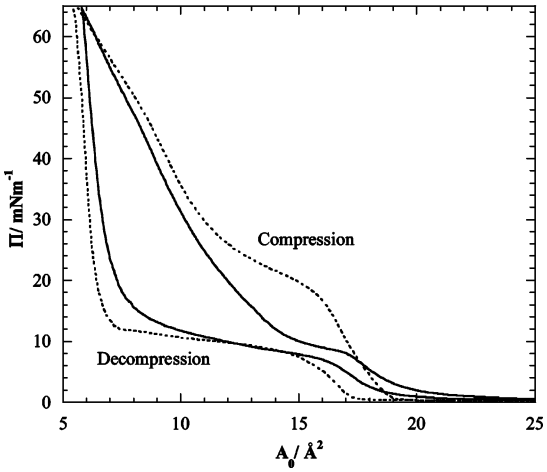

Figure 7. Surface pressure isotherms of p-leu ($\langle M \rangle_{vis}$ = 13.4 kDa) spread on 10 mM NaOH with NaCl added to a total ionic strength of 100 mM (solid trace) and 10 mM NaOH + 10 mM $CaCl_2$ with NaCl added to a total ionic strength of 100 mM (dotted trace).

ionic strength has a pronounced influence on the surface pressure at low degree of compression (A_0 > 20 Å^2; Figure 6). More specifically, the surface pressure of the film is effectively zero when the subphase ionic strength is high. However, at a degree of compression corresponding to an area of ca. 17 Å^2 per amino acid residue, the isotherms in the low- and high-ionic strength cases start to overlap and the surface pressure at the collapse plateau is practically independent of ionic strength. On the neutral subphase, where the peptide is expected to have a zwitterionic character, the effects of ionic strength are more complex. Here, the collapse plateau is lowered upon increasing ionic strength, and the isotherm tails toward larger A_0. The angular dependence observed in CD spectra of LB-films deposited from 100 mM NaCl (Figure 3) is no longer present in the 5 M NaCl case (data not shown).

Since Ca^{2+} is known to bind strongly to carboxylate groups and to form bridges between such moieties, the effect of adding Ca^{2+} to the subphase was investigated. Addition of Ca^{2+} to an alkaline subphase shows that the NaOH effect on the collapse plateau can be reversed by addition of Ca^{2+} (Figure 7). On the other hand, CD data show that addition of Ca^{2+} to the subphase does not affect the peptide conformation. However, the CD spectra of films deposited from the Ca^{2+} containing subphase are dependent on the orientation of the quartz plate in the same way as CD spectra of films deposited from, for example, 100 mM NaCl (Figure 3), indicating a long-range net lateral orientation of the polypeptide strands on the substrate (result not shown).

Finally, the effect of the peptide molecular mass on the compression and decompression isotherm was investigated by comparing the results for 13.4 and 29.4 kDa peptides. For the 29.4 kDa peptide, unlike the 13.4 kDa case, addition of NaOH to the subphase only results in a minor effect on the isotherms (Figure 8). The increase in the peptide molecular mass does not affect the peptide secondary conformation on LB films. However, unlike the 13.4 kDa peptide when spread on NaOH, the orientation of the quartz plate does affect the CD spectra for the 29.4 kDa peptide under the same conditions (results not shown), indicating a long-range net lateral orientation of the polypeptide strands on the substrate. Since the limited solubility of the 29.4 kDa peptide necessitated the use of a spreading solvent more rich in TFA (1:4 TFA:chloroform, rather than 1:20), the influence of solvent composition for the 13.4 kDa peptide was also investigated. The isotherm was unaffected by the TFA:chloroform ratio in the range from 1:4 to 1:20 (data not shown), which confirms the claim that the differences observed between the 13.4 and 29.4 kDa peptides are indeed an effect of peptide molecular mass rather than solvent composition.

Discussion

The only titrating groups on p-leu are the carboxylic and amino terminals. Consequently, the p-leu strands can safely be assumed to be zwitterionic on a pH neutral subphase, with the amino and carboxylic terminals on each strand carrying a positive and negative unit charge, respectively. Similarly, on alkaline and acidic subphases the peptide strands can be assumed to be anionic and cationic, respectively. The fact that isotherms of p-leu show a pronounced pH dependence therefore strongly suggests that peptide end-group charge has a surprisingly large impact on the surface characteristics of hydrophobic peptides (Figures 1, 2). CD spectra substantiate this claim. More specifically, the angular dependence of the CD spectra (Figure 3) implies that the charge of the peptide strands affect the lateral molecular orientation within the monolayer.

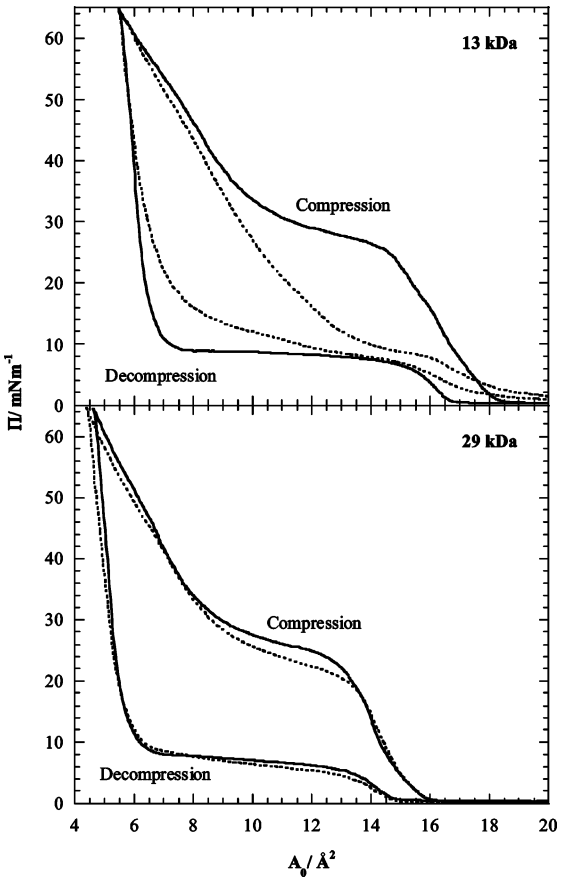

Figure 8. Surface pressure isotherms of p-leu ($\langle M \rangle_{vis}$ = 13.4 and 29.4 kDa) spread on 100 mM NaOH (dotted trace) and 100 mM NaCl (solid trace).

To rationalize the effects, it is helpful to briefly review the general behavior of hydrophobic peptides at the air−water interface. As mentioned in the Introduction, there is compelling evidence that hydrophobic polyamino acids self-assemble into domains at the air−water interface, even at low degrees of compression ($\Pi \approx 0$ mNm^{-1}).[40−44] The present BAM studies verify the formation of peptide domains. Within the domains, hydrophobic, van der Waals, and dipole interactions are all expected to favor structures in which the peptide strands are aligned with their principal axes parallel with each other. This alignment, in turn, would be expected to give rise to a formation of nematic and smectic liquid crystalline phases in two dimensions.[5,7,8,73,74] In the present case, the domain structure is probably nematic since polydisperse systems are unable to adopt a smectic structure in two dimensions.[7,73,74] On the basis of this information, we can now discuss the influence of end-group charge, where we can define five major factors that control the formation of the peptide films:

1. Hydrophobic, van der Waals, dipole−dipole, and other interactions that tend to induce a parallel orientation of peptide strands in aggregates.

2. Electrostatic end-group interactions between peptide strands.

3. Condensation of counterions from the bulk onto charged films, to establish charge neutrality.

4. A finite surface concentration of free peptide strands at low surface pressure is in equilibrium with the peptides in aggregated domains. The layer can be regarded as a quasi-two-phase situation in which the domains are "soluble" at the surface, to a certain extent.

5. The systems are far from equilibrium, as judged from the kinetic investigations and the large hysteresis between compression and decompression isotherms.

Let us first consider zwitterionic strands (neutral pH conditions). In this case, there is an obvious possibility to form ion pairs between neighboring peptide strands. In addition, zwitterionic strands build charge neutral aggregates, which do not induce counterion condensation. Both factors would be expected to promote domain formation and suppress the equilibrium surface concentration of free peptide strands. In the anionic case (alkaline conditions), the possibility for ion pair formation does not exist and domain formation would necessarily induce counterion condensation. Both factors would suppress aggregation and lead to a high surface concentration of free peptide strands. In terms of compression isotherm characteristics, this inferred difference between the neutral and alkaline case would thus lead to a higher surface pressure at low degrees of compression (where the contribution from free peptide strands dominates) in the latter case. This is consistent with the experimental results (Figure 1). Increasing ionic strength decreases the effects of electrostatics, as well as those of counterion condensation. In the alkaline case, increasing ionic strength leaves the collapse plateau unaffected but decreases the surface pressure at low degrees of compression (Figure 6). The former observation suggests that the internal structure of the monolayer prior to the collapse plateau is independent of ionic strength. The latter observation suggests an enhanced domain formation at high ionic strength, consistent with our expectations. For the zwitterionic (neutral pH) case, increasing ionic strength lowers the collapse plateau, suggesting substantial effects on the monolayer structure prior to the collapse plateau. Since there are no counterion effects, the effects must be due to screening of electrostatic interactions between peptide strands. The screening effects that have the most profound effects on film characteristics thus seem to be those between *opposite* charges, since we observe no effects of ionic strength on the surface pressure at the collapse plateau of the anionic film. The data therefore suggest that a decrease of electrostatic *attraction* in the compressed film makes it more prone to collapse, that is, lowers the collapse plateau, whereas a decrease of electrostatic *repulsion* have no obvious impact in this respect.

The pH effects on the isotherm collapse plateau parallel those on the overall molecular orientation in the films, as determined by CD spectroscopy. When interpreting the CD spectroscopic data, we need to keep in mind that we cannot distinguish between results from large individual domains, in the size of the film area analyzed in the CD experiment (4 × 8 mm), and individual domains that fuse to a continuous film during compression. Anyway, the CD data show that the degree of lateral order is higher in the neutral case, where electrostatic attraction prevails. In analogy with the isotherm results, the order proves possible to decrease by decreasing these attractive interactions, either by increasing the ionic strength or by increasing pH.

It would seem that the suggested interplay between electrostatic end-group attraction and lateral molecular order would predict that a decrease in subphase pH (from neutral to acidic) should give rise to the same disordering effect as an increase in subphase pH (from neutral to alkaline). This is, however, not the case. Rather, the peptide behavior on an acidic subphase is nearly identical to that on the neutral one, both in terms of isotherm and CD characteristics. This somewhat unexpected finding is possible to understand from the capacity of carboxylic acids to form strong dimers.[75−77] These interactions yield an

alternative peptide end-group interaction, whose effects are analogous to the effects of electrostatic end-group attraction. The exact same effects can also be achieved under alkaline conditions by addition of calcium ions, which form strong bridges between carboxylate end groups. In conjunction, our data clearly indicate that the effects of subphase characteristics on peptide film behavior are attributable to effects on the effective molecular mass of the peptide strands. More specifically, any mechanism that contributes to a strong interaction between neighboring strands is suggested to increase the tendency for domain formation or domain fusion at $\Pi > 0$ mNm^{-1}. In agreement with these observations, an actual increase of peptide molecular mass gives rise to the exact same ordering effect (Figure 8).

The kinetic data provide an answer to the question whether the observed effects of subphase characteristic are thermodynamic or kinetic in origin or both. The assumptions used to derive eq 3 and the procedure used to refine the parameters k, n, and Π_c do not allow for any detailed, qualitative analysis of the mechanism and subphase influence on the film collapse. However, we may conclude that the kinetic data show excellent agreement with the Avrami equation and that this observation provides strong support for the idea that the film properties at the collapse plateau is strongly affected by nucleation and growth of crystallites. We can also safely use the kinetic data to state that the subphase properties influence not only the kinetic behavior of the films but also their equilibrium properties (more specifically, the limiting surface pressure Π_c). For all systems, the value of the exponent n is <1. According to the theory behind the Avrami equation, this would suggest that the nucleation follows a zero-order rate law and, consequently, is predetermined (as opposed to sporadic). It would also suggest that the growing crystallites in the systems grow in a fractal dimension <1. It is possible that these unusual characteristics are caused by the crystallites being "predetermined" to nucleate and grow at the collision points between the individual domains observed in BAM, around impurities in the film, or even around the Wilhelmy plate. However, a more detailed and conclusive analysis of the kinetics and mechanism of crystallization requires further extensive research and falls outside the scope of the present work.

Finally, the fact that the relaxation can be described by a simple equation is somewhat surprising, considering that the origin of the relaxation would be expected to be a complex combination of molecular relaxation and relaxation of the film as a whole. Monolayer compression and decompression in two directions, as performed with a conventional LB trough, can result in substantial film strain and inhomogeneous monolayer collapse.[78,79] Relaxation of such strains and inhomogeneities would clearly be expected to influence the kinetics as measured in the present work. However, the excellent fit of the relaxation data to eq 3 clearly indicates that the main contribution to the film relaxation is an Avrami-type nucleation and growth of a crystalline film.

Conclusions

Traditionally, the surface arrangement of relatively long, hydrophobic peptides comprising only aliphatic unimers has been regarded as being independent of subphase pH. The present work shows that this is not always true. Compression isotherms of p-leu display clear pH dependence in terms of the molecular area and surface pressure at the monolayer-to-bilayer transition collapse plateau. The effects can be understood from the propensity of peptide helices to self-assemble into nematic or smectic structures at the air−water interface and from the influence of end-group charges on this process. For a given peptide, the exact molecular order in the film is possible to influence by changes in the subphase. Generally speaking, any change in the subphase that promotes an increase of the effective molecular mass of the peptide leads to a higher degree of order in the peptide film (Figure 9). The effective molecular mass can be increased by electrostatic attraction between end groups or by formation of carboxylic acid dimers or calcium bridges between such groups. However, it cannot be increased by screening peptide end-group repulsion. The effects of an increase of the effective molecular mass on peptide behavior exactly parallel those of an increase of the actual molecular mass.

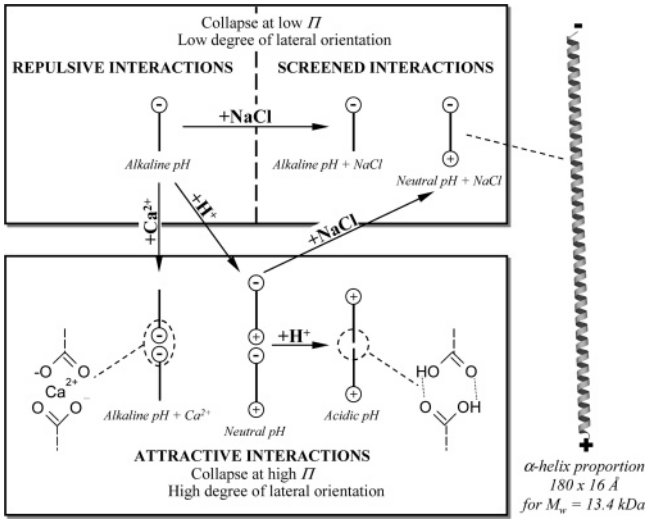

Figure 9. A schematic representation of different ways to influence the effective molecular mass and thereby the degree of lateral surface orientation.

We may conclude that effects of end-group charge can, at least in some cases, be of great importance for peptide behavior at interfaces, even for rather long peptides (more than 100 amino acid residues). The effects increase in importance with decreasing molecular mass and are therefore expected to be of importance for biologically relevant hydrophobic and amphiphilic peptides.

The principles used in the present work to achieve long-range nematic order in peptide films could possibly also be used to obtaining smectic order in monodisperse peptide systems.[1,6,46]

Acknowledgment. Financial support from AstraZeneca R&D Lund and The Swedish Foundation for Strategic Research (Program of Colloid and Interface Technology, SSF) is gratefully acknowledged. Sten Sturefelt is acknowledged for performing the electron microscope and elemental analysis experiment and Marité Cárdenas for help with the BAM experiments. The authors would also like to thank Tommy Nylander for valuable and constructive discussions.

Supporting Information Available: Surface pressure isotherms, repeatability, and peptide subphase losses for p-leu spread on 100 mM NaOH. AFM image of an LB film of p-leu spread on 100 mM NaCl. Surface pressure isotherms and relaxation of p-leu spread on 100 mM NaCl, 100 and 1 mM NaOH. Effect of TFA in the spreading solvent by cholesterol monolayer studies. SEM image of an LB film of p-leu spread on 100 mM NaOH. X-ray spectra of a smooth region and aggregates in an LB film of p-leu spread on 100 mM NaOH.

This material is available free of charge via the Internet at http://pubs.acs.org.

References and Notes

(1) Rapaport, H.; Kjaer, K.; Jensen, T. R.; Leiserowitz, L.; Tirrell, D. A. *J. Am. Chem. Soc.* **2000**, *122*, 12523−12529.

(2) de Witte, P. A. J.; Castriciano, M.; Cornelissen, J. J. L. M.; Scolaro, L. M.; Nolte, R. J. M.; Rowan, A. E. *Chem. Eur. J.* **2003**, *9*, 1775−1781.

(3) Chung, S.-W.; Markovich, G.; Heath, J. R. *J. Phys. Chem. B* **1998**, *102*, 6685−6687.

(4) Schönherr, H.; Paraschiv, V.; Zapotoczny, S.; Crego-Calama, M.; Timmerman, P.; Frank, C. W.; Vancso, G. J.; Reinhoudt, D. N. *Proc. Natl. Acad. Sci. U.S.A.* **2002**, *99*, 5024−5027.

(5) Yang, P.; Kim, F. *ChemPhysChem* **2002**, *3*, 503−506.

(6) Rapaport, H.; Möller, G.; Knobler, C. M.; Jensen, T. R.; Kjaer, K.; Leiserowitz, L.; Tirrell, D. A. *J. Am. Chem. Soc.* **2002**, *124*, 9342−9343.

(7) Yu, S. M.; Soto, C. M.; Tirrell, D. A. *J. Am. Chem. Soc.* **2000**, *122*, 6552−6559.

(8) Kim, F.; Kwan, S.; Akana, J.; Yang, P. *J. Am. Chem. Soc.* **2001**, *123*, 4360−4361.

(9) Sastry, M.; Rao, M.; Ganesh, K. N. *Acc. Chem. Res.* **2002**, *35*, 847−855.

(10) Ghadiri, M. R.; Granja, J. R.; Milligan, R. A.; McRee, D. E.; Khazanovich, N. *Nature* **1993**, *366*, 324−327.

(11) Loi, S.; Butt, H.-J. *Langmuir* **2002**, *18*, 2398−2405.

(12) Collier, C. P.; Saykally, R. J.; Shiang, J. J.; Henrichs, S. E.; Heath, J. R. *Science* **1997**, *277*, 1978−1981.

(13) Tian, Z. R.; Voigt, J. A.; Liu, J.; Mckenzie, B.; Mcdermott, M. J. *J. Am. Chem. Soc.* **2002**, *124*, 12954−12955.

(14) Haldar, D.; Banerjee, A.; Drew, M. G. B.; Das, A. K.; Banerjee, A. *Chem. Commun.* **2003**, 1406−1407.

(15) Loi, S.; Wiesler, U.-M.; Butt, H.-J.; Müllen, K. *Chem. Commun.* **2000**, 1169−1170.

(16) Duan, H.; Chen, D.; Jiang, M.; Gan, W.; Li, S.; Wang, M.; Gong, J. *J. Am. Chem. Soc.* **2001**, *123*, 12097−12098.

(17) Conner, M. D.; Regen, S. L. *Adv. Mater.* **1994**, *6*, 872−874.

(18) Lee, S.; Dutcher, J. R.; Hillebrands, B.; Stegeman, G. I.; Knoll, W.; Duda, G.; Wegner, G.; Nizzoli, F. *Mater. Res. Soc. Symp. Proc.* **1990**, *188*, 355−360.

(19) Nizzoli, F.; Hillebrands, B.; Lee, S.; Stegeman, G. I.; Duda, G.; Wegner, G.; Knoll, W. *Mater. Sci. Eng.* **1990**, *B5*, 173−176.

(20) Mathauer, K.; Mathy, A.; Bubeck, C.; Wegner, G.; Hickel, W.; Scheunemann, U. *Thin Solid Films* **1992**, *210/211*, 449−451.

(21) Mathy, A.; Mathauer, K.; Wegner, G.; Bubeck, C. *Thin Solid Films* **1992**, *215*, 98−102.

(22) Hickel, W.; Duda, G.; Jurich, M.; Kröhl, T.; Rochford, K.; Stegeman, G. I.; Swalen, J. D.; Wegner, G.; Knoll, W. *Langmuir* **1990**, *6*, 1403−1407.

(23) Menzel, H.; Weichart, B.; Hallensleben, M. L. *Thin Solid Films* **1993**, *223*, 181−188.

(24) Mathauer, K.; Schmidt, A.; Knoll, W.; Wegner, G. *Macromolecules* **1995**, *28*, 1214−1220.

(25) Menzel, H.; Hallensleben, M. L.; Schmidt, A.; Knoll, W.; Fischer, T.; Stumpe, J. *Macromolecules* **1993**, *26*, 3644−3649.

(26) Vierheller, T. R.; Foster, M. D.; Schmidt, A.; Mathauer, K.; Knoll, W.; Wegner, G.; Satija, S.; Majkrzak, C. F. *Macromolecules* **1994**, *27*, 6893−6902.

(27) Schmidt, A.; Mathauer, K.; Reiter, G.; Foster, M. D.; Stamm, M.; Wegner, G.; Knoll, W. *Langmuir* **1994**, *10*, 3820−3826.

(28) Motschmann, H.; Reiter, R.; Lawall, R.; Duda, G.; Stamm, M.; Wegner, G.; Knoll, W. *Langmuir* **1991**, *7*, 2743−2747.

(29) Higushi, M.; Koga, T.; Taguchi, K.; Kinoshita, T. *Trans. Mater. Res. Soc. Jpn.* **2002**, *27*, 489−492.

(30) Ulvenlund, S.; Gillgren, H.; Stenstam, A.; Bäckman, P.; Sparr, E. *J. Colloid Interface Sci.* **2001**.

(31) Gillgren, H.; Stenstam, A.; Ardhammar, M.; Nordén, B.; Sparr, E.; Ulvenlund, S. *Langmuir* **2002**, *18*, 462−469.

(32) Birdi, K. S.; Fasman, G. D. *J. Polym. Sci.* **1972**, *10*, 2483−2486.

(33) Malcolm, B. R. *Adv. Chem. Ser.* **1975**, *145*, 338−359.

(34) Auduc-Boyer, N.; Stevenson, I.; Duc, T. M.; Linossier, I.; Gaillard, F. *Surf. Interface Anal.* **1995**, *23*, 673−679.

(35) Baglioni, P.; Dei, L.; Gabrielli, G. *J. Colloid Interface Sci.* **1983**, *93*, 402−410.

(36) Kawaguchi, M.; Tohyama, M.; Mutoh, Y.; Takahashi, A. *Langmuir* **1988**, *4*, 407−410.

(37) Tredgold, R. H.; Jones, R. *Langmuir* **1989**, *5*, 531−533.

(38) Tanizaki, T.; Hara, K.; Takahara, A.; Kajiyama, T. *Polym. Bull.* **1993**, *30*, 119−126.

(39) Lavigne, P.; Tancréde, P.; Larmarche, F.; Max, J.-J. *Langmuir* **1992**, *8*, 1988−1993.

(40) Fukuto, M.; Heilmann, R. K.; Pershan, P. S.; Yu, S. M.; Griffiths, J. A.; Tirrell, D. A. *J. Chem. Phys.* **1999**, *111*, 9761−9777.

(41) Lavigne, P.; Tancréde, P.; Lamarche, F.; Grandbois, M.; Salesse, C. *Thin Solid Films* **1994**, *242*, 229−233.

(42) Malcolm, B. R. *Proc. R. Soc. London, Ser. A* **1968**, *305*, 363−385.

(43) Shuler, R. L.; Zisman, W. A. *Macromolecules* **1972**, *5*, 487−492.

(44) Malcolm, B. R. *Prog. Surf. Membr. Sci.* **1973**, *7*, 183−229.

(45) *The Merck Index*, 13th ed.; Merck & Co., Inc.: Rahway, NJ, 2001.

(46) Kuzmenko, I.; Rapaport, H.; Kjaer, K.; Als-Nielsen, J.; Weissbuch, I.; Lahav, M.; Leiserowitz, L. *Chem. Rev.* **2001**, *101*, 1659−1696.

(47) Gabrielli, G.; Baglioni, P. *J. Colloid Interface Sci.* **1981**, *83*, 221−229.

(48) Baglioni, P.; Dei, L.; Ferroni, E.; Gabrielli, G. *J. Colloid Interface Sci.* **1986**, *109*, 109−114.

(49) Baglioni, P.; Gabrielli, G.; Guarini, G. G. T. *J. Colloid Interface Sci.* **1980**, *78*, 347−355.

(50) Gabrielli, G.; Baglioni, P.; Ferroni, E. *J. Colloid Interface Sci.* **1981**, *81*, 139−149.

(51) Puggelli, M.; Gabrielli, G.; Caminati, G. *Colloid Polym. Sci.* **1989**, *267*, 65−70.

(52) Brown, M. E. *Thermochim. Acta* **1997**, *300*, 93−106.

(53) Rodríguez Patino, J. M.; Rodríguez Niño, M. R. *Colloids Surf., B* **1999**, *15*, 235−252.

(54) Carrera Sánchez, C.; Rodríguez Niño, M. R.; Rodríguez Patino, J. M. *Colloids Surf., B* **1999**, *12*, 175−192.

(55) Carrera Sánchez, C.; de la Fuente Feria, J.; Rodríguez Patino, J. M. *Colloids Surf., A* **1998**, *143*, 477−490.

(56) Rodríguez Patino, J. M.; Rodríguez Niño, M. R.; Carrera Sánchez, C. *Langmuir* **2002**, *18*, 8455−8463.

(57) Lee, K. Y. C.; Lipp, M. M.; Takamoto, D. Y.; Ter-Ovanesyan, E.; Zasadzinski, J. A.; Waring, A. J. *Langmuir* **1998**, *14*, 2567−2572.

(58) Rodger, A.; Nordén, B. *Circular Dichroism & Linear Dichroism*; Oxford University Press: New York, 1997.

(59) Stryer, L. *Biochemistry*, 4th ed.; W. H. Freeman & co: New York, 1995; Chapter 3, pp 45−74.

(60) Davidsson, Å.; Nordén, B.; Seth, S. *Chem. Phys. Lett.* **1980**, *70*, 313−315.

(61) Hay, J. N. *Br. Polym. J.* **1971**, *3*, 74−82.

(62) Avrami, M. *J. Chem. Phys.* **1941**, *9*, 177−184.

(63) Avrami, M. *J. Chem. Phys.* **1939**, *7*, 1103−1112.

(64) Avrami, M. *J. Chem. Phys.* **1940**, *8*, 212−224.

(65) Hoffman, J. D.; Guttman, C. M.; DiMarzio, E. A. *Faraday Discuss. Chem. Soc.* **1979**, *68*, 177−197.

(66) Evans, U. R. *Trans. Faraday Soc.* **1945**, *41*, 365−374.

(67) DiMarzio, E. A.; Guttman, C. M.; Hoffman, J. D. *Faraday Discuss. Chem. Soc.* **1979**, *68*, 210−217.

(68) Guttman, C. M.; Hoffman, J. D.; DiMarzio, E. A. *Faraday Discuss. Chem. Soc.* **1979**, *68*, 297−309.

(69) Hoffman, J. D. *Polymer* **1983**, *24*, 3−26.

(70) Hoffman, J. D. *Polymer* **1982**, *23*, 656−670.

(71) Meares, P. *Polymers: Structure and Bulk Properties*; Van Nostrand: London, 1965; Chapter 5, pp 125−159.

(72) Sperling, L. H. *Introduction to Physical Polymer Science*; 2nd ed.; John Wiley & Sons, Inc.: New York, 1992; Chapter 6, pp 198−278.

(73) Yu, S. M.; Conticello, V. P.; Zhang, G.; Kayser, C.; Fournier, M. J.; Mason, T. L.; Tirell, D. A. *Nature* **1997**, *389*, 167−170.

(74) Bates, M. A.; Frenkel, D. *J. Chem. Phys.* **2000**, *112*, 10034−10041.

(75) Subramanian, S.; Zaworotko, M. J. *Coord. Chem. Rew.* **1994**, *137*, 357−401.

(76) Etter, M. C. *Acc. Chem. Res.* **1990**, *23*, 120−126.

(77) Aakeröy, C. B.; Seddon, K. R. *Chem. Soc. Rev.* **1993**, *22*, 397−407.

(78) Malcolm, B. R. *Thin Solid Films* **1985**, *134*, 201−208.

(79) Malcolm, B. R. *Thin Solid Films* **1989**, *178*, 17−25.